# SOLIDIFYING SESSILE WATER DROPLETS

W.W. Schultz*, M.G. Worster, D.M. Anderson**
*Department of Applied Mathematics and Theoretical Physics, University of Cambridge*
*Silver Street, Cambridge, CB3 9EW, U.K.*
firstauthor@myuniv.edu

* *permanent address: Department of Mechanical Engineering and Applied Mechanics*
*University of Michigan, Ann Arbor, MI 48109-2121, U.S.A.*
** *permanent address: Department of Mathematics*
*George Mason University, Washington DC, U.S.A.*

**Keywords:** sessile droplet, pure water, tri-junction, boundary integral method, macroscopic scale

**Abstract** The form of the solidified product in containerless solidification is sensitive to conditions at the tri-junction between the solid, the melt and the surrounding vapor. We consider experimentally and analytically the simple system of a liquid droplet solidifying on a cold plate. As opposed to the one-dimensional analysis of Anderson et al. (1996), our axisymmetric boundary integral analysis shows that a simple non-dynamic condition at the tri-junction is sufficient. A simple static zero growth angle of zero along with a fluid that expands upon freezing produces a frozen drop that has an inflection point near a cusp that forms at the symmetry axis. Some dynamics of the droplet are considered with discussion of possible micro droplet ejection at the final moment of solidification.

## Introduction

Containerless solidification is one of the most common methods of growing crystals from melts. Many such systems (e.g. Czochralski crystal growth, float-zone processing, and laser welding) have complex geometries with free boundaries that are governed in part by the tri-junction condition, where the solid, its melt, and a vapour phase meet. By influencing the shape of the liquid-vapour meniscus, the tri-junction



*P. Ehrhard et al. (eds.), Interactive Dynamics of Convection and Solidification,* 209–226.

can directly or indirectly (in conjunction with capillary- or buoyancy-driven convection) affect the crystal purity, uniformity and the presence of defects. We simplify the tri-junction conditions (actually, all can be written as a one-parametric family in this case) in a simple model of the solidifying sessile water droplet (figure 1). The curious shape of the solidified water droplet provides a simple test of the tri-junction condition that can be used in theoretical analyses of more complicated systems. We discover that using a more realistic model for the solidifying interface geometry allows a simpler tri-junction model that still compares well with experiments.

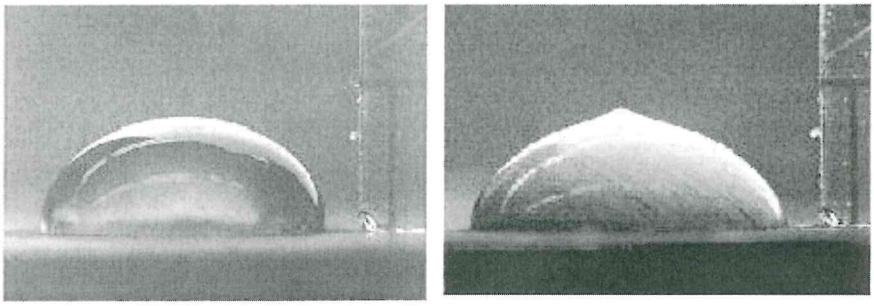

*Figure 1* The initial water droplet and the final frozen form (from Anderson et al. (1996)). The plate is cooled and freezes the droplet from below. The sessile water drop is approximately 4 *mm* high.

We choose to concentrate on the problem of pure water freezing on a perfectly conducting surface for several reasons:

- it provides a simple generic test of contact line models during phase change,
- the large latent heat of the solidification process allows the use of the Laplace equation for the field equation,
- the expansion on freezing allows unusual droplet shapes and kinematics, and
- these unusual shapes may play a very important tribological role for freezing rain on roads or aerodynamic role for freezing rain on wing surfaces.

This study revisits that of Anderson et al. (1996), except that the flat solidifying interface assumption is no longer imposed. The reasons

for relieving the flat interface function are several-fold. The most important is to attempt to fit the data with a simpler tri-junction condition. The relaxation of this restriction is important in that the flat interface assumption violates a local analysis near the tri-junction condition. Additionally, this newer model will allow studying most materials that contract upon solidifying, model possible droplet ejection more accurately, and determine if a crater can form under these conditions.

# 1. PROBLEM FORMULATION

The model geometry follows those of previous authors (Satunkin et al. (1980), Sanz et al. (1987)) and is shown in figure 2. The solidifying droplet is axisymmetric with known initial contact angle $\phi_o$ and liquid volume $\mathcal{V}_o$. We no longer assume the solidification front to be planar as in Anderson et al. (1996). Hence, $\phi$ is no longer the apparent contact angle, although $\phi$ still defines the angle between the horizontal and the tangent to liquid-vapour interface at the tri-junction location.

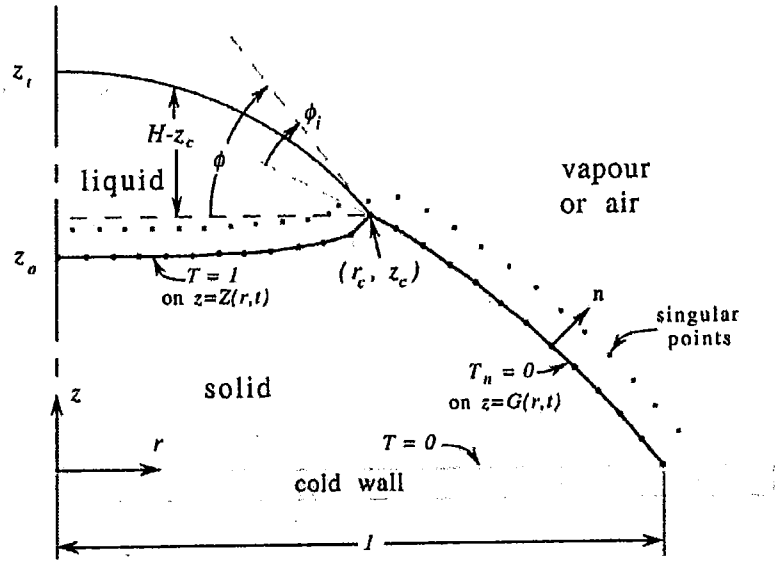


*Figure 2* Problem schematic. All variables are dimensionless. In particular, the wetted drop radius is scaled to unity.

The shape of the solidified droplet is determined by the evolution of the solid-liquid interface location $Z(r,t)$ and the tri-junction position $(R_c, Z_c)$. The tri-junction condition depends on $R_c$ and the volume of the liquid and solid portion of the droplet $\mathcal{V}_l$ and $\mathcal{V}_s$ through a global conservation of mass

$$\rho \mathcal{V}_s + \mathcal{V}_l = \mathcal{V}_o \,, \tag{24.1}$$

where $\rho = \rho_s/\rho_l$ is the solid to liquid density ratio. Hence, $\rho$ is less than 1 for a material that expands, like water. Second, the shape of the liquid-vapour interface, a free boundary subject to the effects of capillarity and gravity, imposes a relation between $r_o$, $\mathcal{V}$ and $\phi$ at the contact (or tri-junction) line. These two relations are sufficient to determine the shape of the solidified droplet once $\phi$ is known. This inclination at the contact line is the focus of our study and is described in the next section.

For simplicity and clarity, we shall focus almost exclusively on the case where gravitational effects are neglected. We assume the freezing of the drop is axisymmetric and choose a coordinate system with its origin on the cold surface with $z$ pointing upwards and $r$ pointing away from the symmetry axis as shown in figure 2.

Length, time, mass, and temperature are scaled by $r_w$, $\rho_s L r_w^2/(k\Delta T)$, $\rho_s r_w^3$, and $\Delta T = T_o - T_m$, respectively. Here $r_w$ is the wetted drop radius, $\rho_s$ is the solid density, $L$ is the specific latent heat, $k$ is the solid thermal conductivity, and $T_o$ and $T_m$ are the cold plate and melt temperature, respectively. We assume that the melt temperature is independent of the interface speed (equilibrium thermodynamics) and surface curvature (no Gibbs Thompson effect). The standard heat equation then becomes the governing (dimensionless) equation

$$T_t + St\, \nabla^2 T = 0\,, \tag{24.2}$$

where the Stefan number $St = L/(c\Delta T)$ is typically very large ($c$ is the specific heat of the solid). The subscripts $r$, $z$, $t$, $n$ represent partial differentiation. In this study, we choose to examine only the case of $St \to \infty$. The resulting Laplace equation is much more amenable to a simple boundary integral analysis.

The boundary conditions are

$$\begin{aligned} T &= 0 \quad \text{on} \quad z = 0\,, \\ T &= 1 \quad \text{on} \quad z = Z(r,t)\,, \quad \text{and} \\ T_n + Bi\, T &= 0 \quad \text{on} \quad z = G(r,t)\,, \end{aligned} \tag{24.3}$$

on the cooling surface, the solidifying interface, and solid-vapour interface, respectively. Here the Biot Number is $Bi = hr_w/k$, where $h$ is the heat transfer coefficient to the vapour region environment that for simplicity is assumed to be at the same temperature as the cold plate. The Biot number is often small and will be set to zero here (although this condition can easily be relaxed). The final boundary condition for the solid region describes the evolution of the solidifying interface:

$$\mathbf{r}_t \cdot \mathbf{r}_n = T_n(z = Z(r,t))\,, \tag{24.4}$$

where $\mathbf{r} = (r, Z(r,t))$ is a position vector on the interface, and $n$ is the distance outwardly normal from the interface. This kinematic boundary condition is a consequence of energy conservation at the interface with phase change without heat loss from the interface to the liquid, which is assumed to be at the melt temperature. The constant of proportionality is unity due to the choice of scaling. It should be noted that $Z$ could become double-valued when $\rho > 1$. This does not cause difficulties because the interface is represented implicitly in the algorithm.

## 2. TRI-JUNCTION CONDITION

The problem formulation requires the description of the local movement of the tri-junction denoted by $(R_c, Z_c)$ in figure 2. As in Anderson et al. (1996), this can be described by referring its movement direction to the angle of the solid-vapour interface or the liquid-solid interface. We define the angle of the liquid-vapour interface compared to the horizontal by $\phi$. However, unlike Anderson et al. (1996), since the solid-liquid interface is no longer horizontal, $\phi$ is not the contact angle. Instead, the contact angle is $\phi + \tan^{-1} Z_r(r = R_c)$. Some experimental evidence and thermodynamic theory suggest (Satunkin et al. (1980), Bardsley et al. (1974), Surek & Chalmers (1975)) that the motion of the tri-junction is determined by the advance angle $\phi_i$, representing the change in slope of the solid-vapour interface to the liquid-vapour interface. Unless otherwise specified, we use a zero advance angle corresponding to a fixed contact line. Then, when the density ratio $\rho = \rho_s/\rho_l = 1$, no fluid motion occurs. Values for $\phi_i$ of 5 to 15 degrees are seen for various solidifying substances.

All tri-junction conditions depend either directly or indirectly on the advance angle $\phi$ at the corner, including when the contact angle is prescribed (see local analysis below). If the Bond number $Bo = \rho_l g r_w^2/\sigma$ is small, where $g$ is the gravitational acceleration and $\sigma$ is the liquid-vapour surface tension), then gravity can be neglected and surface tension requires a spherical cap liquid-vapour interface. Straightforward geometric analysis relates the liquid cap volume $\mathcal{V}_+$, the radius $R_c$ of its base and the apparent contact angle $\phi$ via

$$\mathcal{V}_+ = \frac{2\pi R_c^3}{3} \frac{(1 - \cos\phi)^2 (1 + \frac{1}{2}\cos\phi)}{\sin^3\phi}. \tag{24.5}$$

While in Anderson et al. (1996), $\mathcal{V}_+$ represented the total fluid volume, here $\mathcal{V}_+$ represents the fluid volume above $Z_c$ as shown above the dashed horizontal line in figure 2. Since the fluid-solid interface is nonplanar, $\mathcal{V}_+$ can become negative when $\rho > 1$. This indicates that the liquid-vapour

interface is concave, but (24.5) still holds. $\mathcal{V}_-$ is determined from simple numerical quadrature.

When the Bond number can no longer be considered negligible, $\phi = \tan^{-1}(H_z)$ is determined after the interface shape is numerically integrated from

$$Bo\,(H - Z_c) - p = \frac{1}{r}\left(\frac{rH_r}{(1+H_r^2)^{\frac{1}{2}}}\right)_r , \qquad (24.6)$$

as in Anderson et al. (1996). Here, $p$ is a constant pressure after the hydrostatic term is eliminated. Even a small Bond number expansion requires numerical integration. Some comparisons are made to experiments in this study where the Bond number would have a minor effect. Bond number is set identically to zero since its effect is comparable to the experimental error, and the effects of other assumptions here (specifically the assumption of an adiabatic solid-vapour interface).

## 3. LOCAL ANALYSES

Several local solutions will aid the computational analysis. These include an analysis near the tri-junction line, and the behaviours for small and late time.

### 3.1. HEAT FLOW AT TRI-JUNCTION CONDITION

Since the tri-junction condition is important to the ultimate shape of the frozen droplet, an examination of the heat flow near this location is appropriate. The local solution near the contact line can be considered to be planar except when $r_c \to 0$. A local schematic near the tri-junction condition is shown in figure 3. A local $(r', \theta')$ polar coordinate system is centered at the tri-junction $(R_c, Z_c)$ with $\theta'$ measured from the solid-vapour interface toward the solid-liquid interface at $\theta' = \alpha$.

The solution for the resulting local Laplacian operator is of the form $T = r^\lambda f(\theta')$. The Neumann boundary condition at $\theta = 0$ and the inhomogeneity of the Dirichlet condition are satisfied by

$$T = r^\lambda \cos\lambda\theta' + 1\,, \qquad \text{as} \quad (r,z) \to (R_c, Z_c)\,, \qquad (24.7)$$

where the most dominant behaviour is for $\lambda = \pi/(2\alpha)$. For acute angles $\alpha < \pi/2$, $\lambda$ is less than unity, and the infinite flux at the corner leads to more rapid solidification causing $\alpha$ to grow. Obtuse angles lead to $\lambda > 1$, where heat flux and hence solidification rate increase from the corner, causing $\alpha$ to decrease. In other words, the model cannot support a singularity and hence a heat flux line (adiabatic surface or in this case,

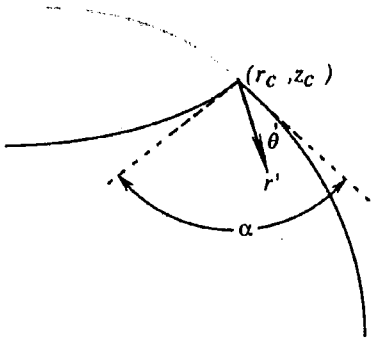


*Figure 3* Local analysis.

the solid-vapour interface) is orthogonal to an isotherm (the solid-liquid interface). Hence $\alpha = \pi/2$, and the simple solution of the flat interface of Anderson et al. (1996) leads to a contradiction locally.

The corner angle $\alpha = \pi/2$ has other implications. It means that there is a simple relationship between the growth angle and the contact angle. The contact angle becomes $\phi' + \pi/2$. Hence, the pinned contact line condition corresponds to a 90-degree contact angle.

On the other hand, the isothermal cold wall can support a singularity (infinite heat flux) at $(r, z) = (1, 0)$ if the wall has very large thermal conductivity. Then the temperature field is singular when $\phi(r = r_w)$ is not $\pi/2$. This is evidenced by the isotherms not being orthogonal to the adiabatic surface (heat flux line). This leads to computational difficulties that will be discussed later.

## 3.2. SMALL TIME BEHAVIOUR

For small time after the drop has hit the surface, the solidifying interface is very close to the cold surface leading to rapid heat transfer and growth of the solid ice layer. Our computations must start with an initial condition that already has a small but finite-thickness solidifying interface. A planar solidifying layer grows with the square root of time (Worster (2001)). For small time, the solidifying surface is nearly parallel to the cold wall. From the previous local analysis at the tri-junction line, the solid-liquid interface would have to quickly adjust to meet the adiabatic solid-vapour interface orthogonally. We have formulated a simple initial interface condition such that

$$Z = Z_o + (Z_c - Z_o)\{\exp[b(r - R_c)] + \exp[-b(r + R_c)]\}\,, \qquad (24.8)$$

where $Z_c$ and $Z_o$ are chosen to approximate the edge and center heights of the solidifying layer, and $b$ is chosen to satisfy the orthogonality condition at the adiabatic surface. This form also satisfies the smooth axisymmetry condition at $r = 0$. Initially, $bR_c \gg 1$, and hence the interface is nearly flat away from the corner and $Z_o$ is a good approximation for $Z$ at $r = 0$. While (24.8) is not a similarity solution, our computations will show that the final solution is relatively independent of the parameters in (24.8) if the initial solidified region is small. This independence is important because a small-time solution would not be a good model of the experimental drop application process. In this sense, the focus of this paper is different than the early freezing process while the drop is still spreading of Schiaffino & Sonin (1997).

## 3.3. LATE TIME BEHAVIOUR NEAR TOTAL SOLIDIFICATION

When the droplet has nearly solidified, the solidification rate again is large as the interface area shrinks to zero. Then the assumption of a quasi-static liquid and equilibrium thermodynamics may no longer be justified. Also, the assumption that all heat flows into the solidifying interface without escaping to the environment becomes more questionable. If the solidifying surface develops a cone ($\phi > 0$ as $R_c \to 0$), this problem is similar to that of the last moments of spherically symmetric freezing drop as studied by Soward (1980). This is owing to the adiabatic surfaces emanating radially from the cone apex. Hence the fluid-solid interface is expected to become spherical as $R_c \to 0$.

Here we examine the problem more simply and assume either a planar or spherical interface and assume a cusp forms so that a local analysis can be found. These two shapes are appropriate to examine because the interface starts out nearly flat and stays fairly flat for much of the solidifying process. In the latter stages, the interface becomes spherical with intermediate stages that look like ellipsoids with varying aspect ratios although we examine only the two limiting cases here.

There are three volumes to consider as shown in figure 4: $\mathcal{V}_+$ for the liquid spherical cap volume above $Z_c$, $\mathcal{V}_-$ for that of the liquid reservoir below $Z_c$ (for a spherical liquid-solid interface, and $\mathcal{V}_s$ for the portion of the sphere with solid angle $\theta$ (or cone above $Z_c$ and the spherical cap $\mathcal{V}_-$). The volume $\mathcal{V}_+$ is found from (24.5) with $\phi$ replaced by $\frac{\pi}{2} + \phi_i - \theta$. Since the liquid-solid interface must be orthogonal to the conical surface, $\mathcal{V}_-$ is found from (24.5) with $\phi$ replaced by $\theta$.

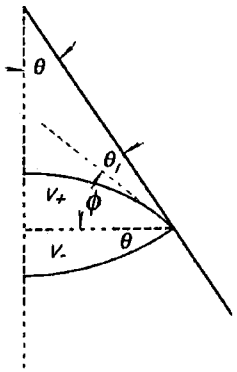


*Figure 4* Cone formation geometry.

Here $\theta = \pi/2 - \phi + \phi'$ as $r \to 0$. We simply use conservation of mass (24.1) and include $\mathcal{V}_-$ for the flat interface case and $\mathcal{V}_-$ as a liquid for the spherically-shaped interface. The results are shown in figure 5.

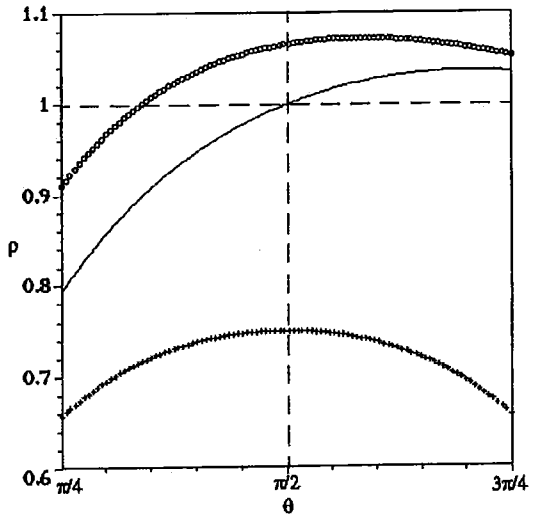


*Figure 5* Cusp angle formation as a function of density ratio. The curve made of closely spaced plus signs is the flat interface model and is identical to a portion of the dashed line of figure 4 in Anderson et al. (1996). The solid line and that line composed of circles are for the spherically-shaped interface with growth angle $\phi'$ of 0 and 10 degrees, respectively. Note that conical peaks are predicted when $\theta < \pi/2$ and conical dimples are predicted for $\theta > \pi/2$. For the case with $\phi' = 0$ (the fixed contact line condition), this transition from dimples to peaks occurs exactly at $\rho = 1$.

We assume: 1) that the solid-vapour interface is adiabatic, 2) the specific heat of the solid is negligible compared to the latent heat, and 3) the heat transfer at the cold plate is relatively constant in the final short moments of the freezing process. Hence the heat flux to the solidifying interface is constant as is the volumetric solidification rate. This leads to

$$Z_{b_t} = const(Z_b - Z_a)^{-2} , \tag{24.9}$$

where $Z_a$ is the ultimate cone apex location. If the liquid volume is proportional to $(Z_b - Z_a)^3$ or $R^3$ where $R$ is an effective "drop radius", the kinetic energy of the liquid (proportional to volume times speed squared) increases as the drop radius decreases like $1/R$. Hence eventually, there could be enough energy to convert into the extra surface tension energy caused by drop detachment that would be proportional to $R^2$. However, it would seem that sudden deceleration of the solidification would be necessary to catapult, rather than bin the drop to the solid. It is also likely that surface contamination would play an important role in the final moments[1].

# 4. NUMERICAL METHOD

## 4.1. AXISYMMETRIC BOUNDARY INTEGRAL METHOD

When the time dependent term in the heat equation can be ignored, the resulting Laplacian equation can be readily handled by boundary integral techniques. The free space three-dimensional Green's function is

$$G = \frac{1}{4\pi|\mathbf{r} - \mathbf{r}_o|} , \tag{24.10}$$

where $\mathbf{r}$ is the evaluation point and $\mathbf{r}_o$ is the singular location. Then Green's identity gives an integral equation

$$\frac{\alpha}{2\pi} T(\mathbf{r}_o) = \int T G_n - T_n G \, dS , \tag{24.11}$$

where the integration is principal valued over the boundary of the solution domain and $\alpha$ is the solid angle of the surface at $\mathbf{r} = \mathbf{r}_o$.

The axisymmetric problem can be integrated analytically in the azimuthal direction to give (Zhou & Graebel (1990))

$$\frac{\alpha}{2\pi} T(\mathbf{r}_o) = \int T J_n - T_n J \, dS , \tag{24.12}$$

where

$$J = \frac{-rK(m)}{\pi[(r + r_o)^2 + (z - z_o)^2]^{1/2}} \tag{24.13}$$

to form a principal-valued line integral instead of the surface integral and $\alpha$ is the included angle equal to $\pi$ except at corners of the domain. Here, $\mathbf{r}_o = (r_o, z_o)$ and $K$ is the elliptic integral as defined by Abramowitz & Stegun (1970) with argument $m$ given by

$$m = \frac{4rr_o}{[(r+r_o)^2 + (z-z_o)^2]} \,. \tag{24.14}$$

Solving (24.12) also requires the gradient of $J$ that becomes

$$\begin{aligned} \nabla J = & \frac{1}{\pi[(r+r_o)^2 + (z-z_o)^2]^{3/2}} \times \\ & \left[ \frac{E(m)}{(1-m)} \frac{r^2 - r_o^2 - (z-z_o)^2}{2} \right. \\ & \left. + \frac{(r+r_o)^2 + (z-z_o)^2}{2} K(m) \,,\, \frac{E(m)}{(1-m)} r(z-z_o) \right] \,. \end{aligned} \tag{24.15}$$

The modified Green's function $J$ has a logarithmic singularity as $\mathbf{r} - \mathbf{r}_o \to 0$. The singularity of $\nabla J$ is greater, but the expected $1/|\mathbf{r} - \mathbf{r}_o|$ singularity does not contribute except at corners of the contour integral.

The contour integral in (24.12) can be limited to the solid-vapour and the liquid-vapour interfaces if images are used to automatically satisfy the Dirichlet boundary condition at $z = 0$. This is accomplished by adding a term identical to $J$ with $\mathbf{r}_o = (r_o, z_o)$ replaced by $(r_o, -z_o)$.

The evaluation of any traditional boundary integral is complicated by the integration of the singular kernels. Numerical evaluation of the singular terms is insufficiently accurate so that analytic subtraction of the singularity is usually required. This analysis is tedious, especially when the singularity is subtracted out globally instead of just locally within one mesh spacing of the singularity. A global subtraction is desirable because mesh refinement will mean that the integration will be nearly singular for several mesh points about the singularity. We had developed a boundary integral method with local singularity subtraction, but a more global approach turned out to be very complicated and had too many special cases (depending on various branch cuts, etc.) to be implemented successfully in an algorithm. The method with local singularity subtraction turned out to be first-order accurate for very simple test cases: a linear temperature profile in the axial direction for a cylindrical domain.

## 4.2. DESINGULARIZED METHOD

Since our problem (considering the local analysis above) is not singular with the possible exception at wall-ice-vapour triple point at $\mathbf{r} = (1, 0)$,

a simpler method is suggested. The standard boundary integral method can be thought of as a continuous distribution of sources $G$ and dipoles $\nabla G$ on the contour. If the solution is not expected to be singular, this distribution can be moved away from the contour outside of the solution domain. Once these singularities are away from the contour, it is nearly equivalent to consider them as point sources so that integration is replaced by simple summation.

This technique has been used successfully for some time in two- and three-dimensions (von Kàrmàn (1930)). A desingularized solution method can involve systematically placing the singularities just outside the solution domain (Webster (1975)) or having the singularity location determined as part of the solution (Han & Olson (1987)). This second approach makes the solution of the potential problem nonlinear and hence less attractive. Instead we will use a method similar to that in Cao et al. (1991) that places the singularities outside the domain that are proportional to the local mesh spacing.

Here, the singularity is an axisymmetric ring source and its image. The solution is then constructed using the singularity in (24.13)

$$T = \sum_{i=1}^{N} a_i \left[ \frac{-rK(m)}{\pi[(r+r_{0i})^2 + (z-z_{0i})^2]^{1/2}} + \text{image} \right] . \tag{24.16}$$

The normal derivative can be formed from the gradient as found in (24.15). We form an $N$ by $N$ algebraic system by evaluating known quantities at $N$ locations along the solid-vapour ($T_n$) and solid-liquid ($T$) interfaces to find the unknown source strengths $a_i$. Then, the unknown quantities of the interface can be determined *a posteori.* In fact, it is possible and sometimes desirable, to form an over-determined system by adding more evaluation points while keeping the number of singularities constant.

The location of the singularities is important and requires careful study. We have opted to place one for each node point on the contour. We place them on the perpendicular bisectors between adjacent nodes, at a distance

$$d = l_d \Delta S \tag{24.17}$$

away from piecewise-linear representation of the contour as shown in figure 2. An additional singularity is placed at the midpoint of the two singularities closest to the corner at $(R_c, Z_c)$ to keep the system determinant since we know both a Dirichlet and Neuman condition at the corner.

In keeping with the approach of Cao et al. (1991), we increase $l_d$ with refinement to ensure proper "quadrature" by the summation procedure.

A simple evaluation of the very simple test case with a linear temperature profile in the axial direction for a cylindrical domain showed exponential accuracy with mesh refinement, especially with large desingularization distances. This is to be expected as one can solve the test case singularity (and its image) if it is placed a large distance above the cylinder.

A more realistic test case involves a contour similar to that found during a simulation. We have determined that the expression (24.8) is a fair representation of the interface for much of the freezing process. We started out with $A = 0.5$ and $\rho = 1$ and found that appropriate values approximately halfway through the freezing process were $Z_c = 0.05$, $Z_o = 0.02$ ($b$ determined from the orthogonality condition) fit the interface contour with minimal error.

Since the solution of the differential equation is "exact", the accuracy of the method can be measured by determining the error in satisfying boundary conditions on the boundary other than at collocation points (where the error should be zero if $M = N$). Naturally, an overdetermined method would minimize this "residual", and we found it to be the case here. However, the accuracy change was minimal and it turned out to cause a zigzag instability in the time-marching program later. Since the time-marching solution is most critically affected by errors near $(R_c, Z_c)$, we used the boundary condition error at the midpoint between the corner node and an adjacent node on the adiabatic or solidifying interface. We found that this convergence was roughly fourth order.

## 4.3. TIME INTEGRATION AND NODAL MOVEMENT

We use a standard fourth-order Runge-Kutta algorithm to march the resulting system of ordinary differential equations for updating the solidifying interface. The boundary condition effectively only determines the normal component of nodal movement, except for the tri-junction node that has an extra condition.

It was important to have a tangential component to this movement in order to keep constant nodal spacing on that surface. Rather than move the nodes on the solid-vapour surface in a similar fashion, we found that it was better to keep these nodes stationary and then add one node for each time step at the tri-junction point.

Numerical integration of the drop volume showed that mass was conserved to within one part in $10^5$. The time step was chosen so that nearly all of this error was due to special discretization.

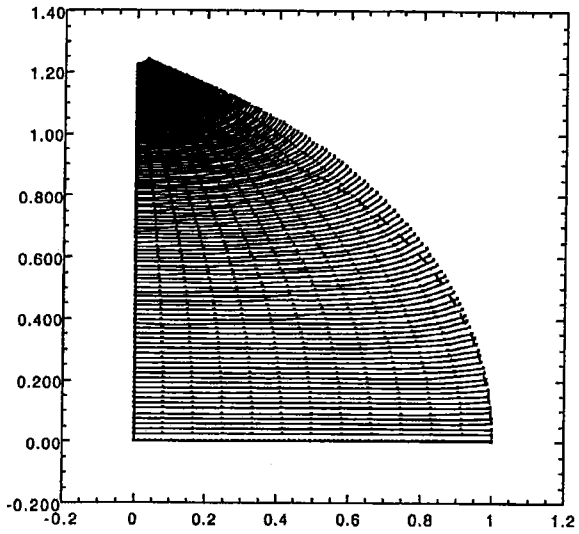


*Figure 6* The shape of the solidifying droplet when $\rho = 0.9$, $A = 1$. The dashed line shows the droplet shape if $\rho = 1$.

## 5. NUMERICAL RESULTS

Figure 6 shows a typical computation for a drop that starts as a hemispherical sessile drop and expands upon freezing. What is shown is a time sequence of solid-liquid interfaces from the centerline to the triple point. We see that the shape of the solidified droplet (as shown by the history of triple point locations) forms a cusp, with the angle of the solid-vapour interface approaching a constant for late times when the droplet is nearly solidified. The computations become difficult as the node spacing on the liquid-solid interface becomes small for late time.

Figure 7 is a similar curve except the original aspect ratio is $A = 0.5$, that is the initial height of the sessile drop is one-half its radius. This shows that the liquid-solid interface stays nearly flat for much of the freezing process. However, it always curves upward near the triple point so that it satisfies the local condition there. This too, approaches a cusp with constant angle at late times. Figure 8 is an enlargement of the cusp region shown in figure 7. This shows that the liquid-solid interface approaches a spherical cap shape at late times when a cusp forms. A similar figure when a cusp does not form ($A = 0.5$, $\rho = 1, \phi = 0$ is not shown, but the surface appears to form an ellipsoid with an aspect ration of approximately 2.5.

The drop kinematics are shown in figure 9 as a function of time. The vertical derivatives of the top of the drop, the base of the liquid drop,

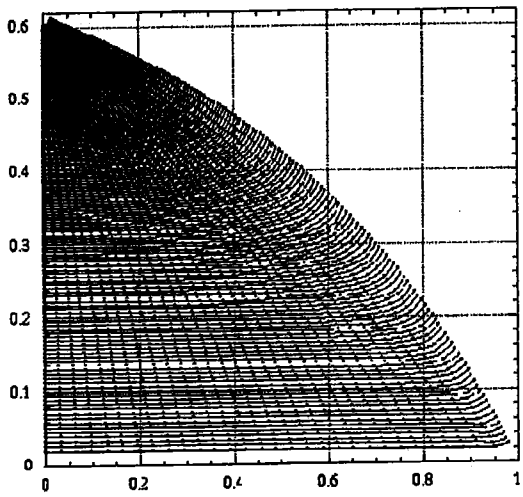


*Figure 7* The shape of the solidifying droplet when $\rho = 0.9$, $A = 0.5$.

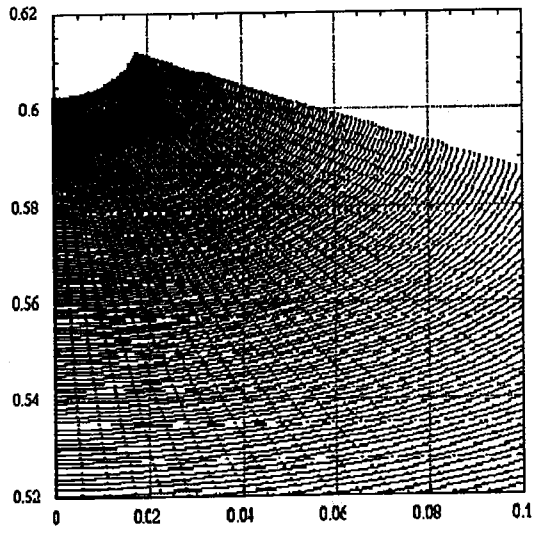


*Figure 8* A close-up of the apex in figure 7 shows that the solidifying interface is nearly spherical when a cusp forms.

and the triple point ($\dot{Z}_t$, $\dot{Z}_o$, $\dot{Z}_c$, respectively) are shown along with the asymptotic trends predicted in sections 3.2 and 3.3. The vertical velocities of each point becomes infinite at $t = 0$ and at the final moment of freezing.

Dimples can form if the material contracts upon freezing $\rho > 1$ (figure 10) or if the growth angle is negative (figure 11). These computations

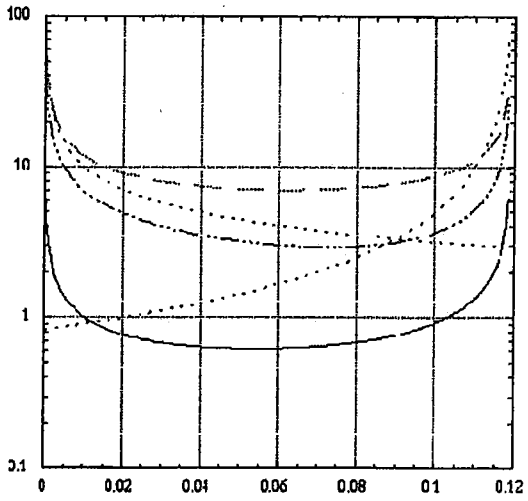


*Figure 9* The drop kinematics are represented by the velocities —— $\dot{Z}_t$, - - - $\dot{Z}_c$, and — - - - — $\dot{Z}_0$. The dotted curves represent asymptotic trends for small $t = 0$ and late $t \approx 1.2$ time for the data of figure 7.

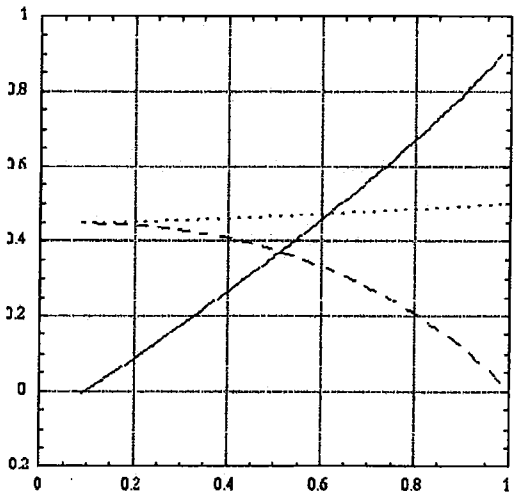


*Figure 10* Corner Coordinates versus $R_c$ for $A = 0.5$ and $\rho = 1.05$. —— $\phi$, - - - $Z_c$, $\cdots$ $Z_t$. The extrapoloation of the angle to $R_c = 0$ shows that a dimple can form.

are even more difficult at late time than those that form a dimple. The dimple is not that pronounced, but can be seen by extrapolating the curve for $\phi$ to $r = 0$.

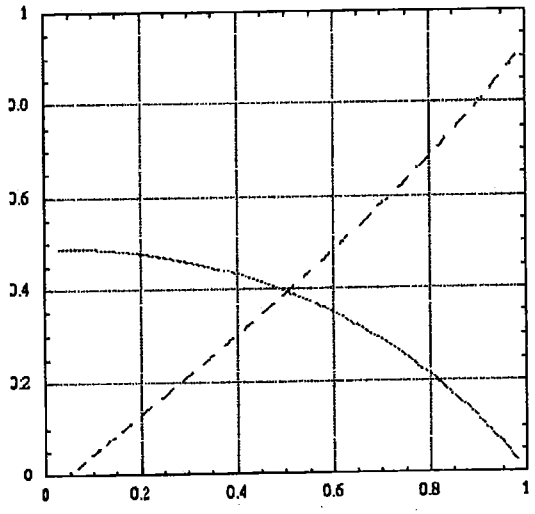


*Figure 11* Corner Coordinates for $\rho = 1$ and $\phi = -0.1$ versus $R_c$ for $A = 0.5$. - - - $\phi$, — $Z_c$. The extrapoloation of the angle to $R_c = 0$ shows that a dimple can form.

## 6. CONCLUSIONS

The following are the conclusions for the simple tri-junction condition of constant growth angle (usually $\phi = 0$):

- Cusps form when the flat interface assumption relaxed and instead computed with an axisymmetric model for either of two cases: the density ratio $\rho < 1$ (as in water) or when the growth angle $\phi_i > 0$ (which may be unphysical).
- A dimple can form for opposite case for either $\rho$ or $\phi_i$.
- Dropping the flat solidifying interface assumption causes the solid-vapour and solid-liquid interface to meet at right angles at the contact line, effectively eliminating the heat-transfer contradiction of the earlier model.
- The interface is fairly flat early, and inflexion points occur late, near the axis of symmetry when $\rho < 1$.
- When a cusp forms at late time for water, a conical approach of the solid-vapour surface forms with a spherical cap solidifying interface.
- Flat and dimpled droplets have ellipsoidal interfaces. For $\rho = 1$, this ellipsoid has 2.5 for major to minor radii.

- An experimental comparison can be made with Anderson et al. (1996) by setting $A = 0.46$, $\rho = .917$ leads to $z_t = .56$ in agreement with the data. The inflection point is also well described.
- Possible micro-droplet ejection is beyond the scope of this model. However, energy arguments indicate droplet ejection is possible.

## Notes

1. Private communication, M. Glicksman (2000)

## References

Abramowitz, M., Stegun, I.A. (eds.) *Handbook of Mathematical Functions*, National Bureau of Standards (1970).

Anderson, D.M., Worster, M.G., Davis, S.H. *J. Cryst. Growth* **163** (1996) 329–338.

Bardsley, W., Frank, F.C., Green, G.W., Hurle, D.T.J. *J. Cryst. Growth* **23** (1974) 341–344.

Cao, Y., Schultz, W.W., Beck, R. *Int. J. Num. Meth. Fluids* **12** (1991) 785–803.

Han, P.S., Olson, M.D. *Int. J. Numer. Meth. Eng.* **24** (1987) 1187–1202.

von Kàrmàn, T. NACA Technical Memorandum No. 574 (1930).

Sanz, A., Meseguer, J., Mayo, L. The influence of gravity on the solidification of a drop, *J. Crystal Growth* **82** (1987) 81–88.

Satunkin, G.A., Tatarchenko, V.A., Shaitanov, V.I. *J. Cryst. Growth* **50** (1980) 133–139.

Schiaffino, S., Sonin, A.A. Motion and arrest of a molten contact line on a cold surface: an experimental study, *Phys. Fluids* **9** (1997) 2217–2226.

Soward, A.M. *Proc. Roy. Soc. Lond.* **A 373** (1980) 131–147.

Surek, T., Chalmers, B. *J. Cryst. Growth* **29** (1975) 1–11.

Webster, W.C. *J. Ship Res.* **19** (1975) 206–218.

Worster, M.G. *Fluid Mechanics of Solidification*, in press (2001) 329–338.

Zhou, Q.N., Graebel, W.P. Axisymmetrical draining of a cylindrical tank with a free-surface, *J. Fluid Mechanics* **221** (1990) 511–532.